Structural Determinants of Signal Speed:

A Multimodal Investigation of Face Processing in Autism Spectrum Disorder

Campbell R. Coleman[*,1], Madelyn G. Nance[*,1], Zachary Jacokes[2], T. Jason Druzgal[3], Vardan Arutiunian[4], Anna Kresse[4,8], Catherine A.W. Sullivan[5], Megha Santhosh[4], Emily Neuhaus[4,6,7], Heather Borland[4], Raphael A. Bernier[6], Susan Y. Bookheimer[9,10], Mirella Dapretto[9,10], Allison Jack[11], Shafali Jeste[12], James C. McPartland[13], Adam Naples[13], Daniel Geschwind[9,10,14,15], Abha R. Gupta[5,13,16], Sara Jane Webb[4,6,7], Kevin A. Pelphrey[1], John Darrell Van Horn[2,17], Benjamin T. Newman[+,3,17], & Meghan H. Puglia[+,1]

on behalf of the ACE GENDAAR Consortium

[+]Correspondence:

Benjamin T. Newman
University of Virginia
Departments of Psychology and
Radiology & Medical Imaging
409 Lane Rd. MR4
Charlottesville, VA 22908
btn6sb@virginia.edu

Meghan H. Puglia
University of Virginia
Department of Neurology
P.O. Box 800883
Charlottesville, VA 22908
meghan.puglia@virginia.edu

*,+ authors contributed equally

[1] Department of Neurology, University of Virginia, Charlottesville, VA

[2] School of Data Science, University of Virginia, Charlottesville, VA

[3] Department of Radiology and Medical Imaging, University of Virginia, Charlottesville, VA

[4] Center for Child Health, Behavior, and Development, Seattle Children's Research Institute, Seattle, WA

[5] Department of Pediatrics, Yale School of Medicine, New Haven, CT

[6] Department of Psychiatry and Behavioral Sciences, University of Washington, Seattle, WA

[7] Institute on Human Development and Disability, University of Washington, Seattle, WA

[8] Peabody College of Education and Human Development, Vanderbilt University, Nashville, TN

[9] Center for Autism Research and Treatment, Semel Institute for Neuroscience and Human Behavior, David Geffen School of Medicine, University of California, Los Angeles, CA

[10] Department of Psychiatry and Biobehavioral Sciences, Semel Institute for Neuroscience and Human Behavior, David Geffen School of Medicine, University of California, Los Angeles, CA

[11] Department of Psychology, George Mason University, Fairfax, VA

[12] Department of Neurology, Children's Hospital of Los Angeles, Los Angeles, CA

[13] Yale Child Study Center, Yale School of Medicine, New Haven, CT

[14] Department of Neurology, David Geffen School of Medicine, University of California Los Angeles, Los Angeles, CA

[15] Department of Human Genetics, David Geffen School of Medicine, University of California Los Angeles, Los Angeles, CA

[16] Department of Neuroscience, Yale School of Medicine, New Haven, CT

[17] Department of Psychology, University of Virginia, Charlottesville, VA

Abstract

Face perception is fundamental to social cognition and often disrupted in autism. However, the neurological basis for this disrupted face perception and the mechanisms underlying altered electrophysiological signaling in autism, such as increased latency of the N170—an electrophysiological marker of face processing, remain unknown. Here, we leverage multimodal neuroimaging in autistic adolescents to establish a link between MRI-measured axonal microstructure within the face processing network and EEG-measured N170 latency. We demonstrate that a novel metric of axonal signal transit time derived from axonal diameter, myelination, and length—estimated axonal latency (EAL)—predicts N170 latency during face processing. Moreover, we demonstrate that individuals with and without autism rely upon different pathways, providing a structural account for autism-related face processing differences. By establishing this relationship between EEG-based electrical function and MRI-based axonal microstructure, we provide a non-invasive, spatially-detailed estimate of neuronal processing speed that can inform understanding of brain function, development, and disorder.

Introduction

The ability of neurons to communicate efficiently is fundamental to brain function, with action potential transmission serving as the primary mechanism for neuronal signaling[1]. At every level—cellular, circuit, and system—this process shapes cognition and behavior by enabling the rapid integration of sensory input. The speed of action potential transmission is largely determined by axonal structure, with myelination and fiber size playing critical roles in reducing electrical resistance and optimizing signal conduction[2,3]. These structural features are essential for neurodevelopment and are frequently altered in neurodevelopmental[4] and neurological disorders[5], including autism spectrum disorder (ASD)[6–8].

Despite decades of research in animal models demonstrating the relationship between axonal structure and neuronal function[9,10], this connection has not been systematically explored in the human central nervous system. Understanding this relationship *in vivo* is particularly crucial for ASD, where differences in white matter development have been implicated in disrupted neural processing[11]. Here, we leverage multimodal neuroimaging in adolescents with and without ASD to establish a link between white matter microstructure—measured via diffusion magnetic resonance imaging (dMRI)—and neuronal signal speed—measured via electroencephalography (EEG). By integrating these two methodologies, we introduce a non-invasive means of estimating action potential transmission across different brain regions and provide a novel framework for investigating individual differences in cognitive processing speed in autistic individuals.

EEG is widely used to study neural activity with high temporal precision, commonly through event-related potentials (ERPs), which capture stereotyped neural responses to sensory

and cognitive stimuli[12]. However, while EEG excels in capturing the timing of signal transmission, it provides little insight into the underlying structural integrity of the white matter pathways responsible for transmitting these signals[13]. Conversely, magnetic resonance imaging (MRI) provides high-resolution structural information but lacks the temporal specificity to assess neuronal function directly[14]. Multimodal neuroimaging approaches combining EEG and MRI capitalize on the strengths of both techniques, offering an unprecedented opportunity to link neural structure to function at the systems level in the human nervous system[15,16]. In this study, we introduce a novel imaging metric, estimated axonal latency (EAL), which translates diffusion-based measures of axonal geometry into an estimate of neuronal conduction transit time. By applying this metric to ASD, we provide a new lens to examine the neural basis of processing speed differences that emerge during development and in neurodevelopmental disorders.

EAL builds upon the established concept of g-ratio, a voxel-wise measure derived from dMRI that reflects the ratio of inner axonal diameter to total axonal diameter[17]. This metric encapsulates the contributions of both myelin thickness and axonal diameter—key determinants of signal conduction efficiency[18]. G-ratio can be mathematically transformed into aggregate conduction velocity[19], a large-scale approximation of neuronal action potential speed. By integrating these diffusion-based measures with white matter tract length estimates, we introduce EAL as a novel marker of neural processing duration, providing a non-invasive alternative to traditional electrophysiological techniques. Importantly, by applying this approach to adolescents with and without ASD, we explore how differences in axonal structure may underlie variations in cognitive processing time that occur with development and disorder.

To demonstrate the utility of EAL, we examine its relationship to electrophysiological latency in face processing, a well-defined cognitive function with direct relevance to ASD. Face perception is a foundational aspect of human social cognition[20,21], and its disruption is frequently observed in autism[22]. A key neural marker of face processing is the N170 ERP, a stereotyped electrical response, typically enhanced for faces, that occurs approximately 170 milliseconds after stimulus onset[23–25]. N170 latency decreases with age, reflecting increasing neural efficiency[26], but differs in autistic individuals[27,28], where processing speed variations have been linked to social-cognitive differences[29]. While previous explanations have attributed these ASD-related N170 latency differences to alterations in visual attention or broader cognitive delays[30,31], these accounts do not address the potential role of underlying white matter structure in shaping signal latency.

Here, we investigate the relationship between N170 latency and EAL along two white matter pathways commonly associated with face processing[32,33] and putatively implicated in N170 signal generation via the ventral visual processing stream[34,35]: the primary visual cortex to right fusiform gyrus (V1-rFG) and the primary visual cortex to right posterior superior temporal sulcus (V1-rpSTS). By linking EAL to an established electrophysiological biomarker of face processing, this study provides a critical bridge between structural and functional aspects of neural processing. Our findings advance our understanding of how white matter microstructure contributes to cognitive function and offer a promising framework for identifying biologically grounded, individualized markers of processing time.

Results

As part of a multisite National Institute of Health sponsored Autism Center for Excellence Network, 125 adolescents (Table 1) underwent comprehensive phenotyping, EEG, and structural and diffusion MRI. While undergoing EEG, participants were presented with faces and symbols as feedback on their performance during an implicit learning task[36]. After preprocessing the EEG data[37], we computed N170 latency as the negative peak latency occurring 170-270 ms after stimulus onset (Fig. 1A) in posterior/occipital channels over the right hemisphere (Fig. 1B) for each condition (faces, symbols). Participants also underwent diffusion, T1-weighted, and T2-weighted imaging. Resulting images were processed per the protocol described in Newman et al.[6]. We defined V1, rFG, and rpSTS regions of interest (Fig. 1C) using the term-based meta-analytic approach available via NeuroSynth.org, and investigated tractograms along the V1-rFG and V1-rpSTS pathways (Fig. 1D). We then generated aggregate g-ratio and aggregate conduction velocity maps for each of our pathways of interest (Fig. 1E), and computed EAL for each pathway by dividing aggregate conduction velocity by tract length.

To establish EAL as a metric of signal latency, we built models predicting N170 latency to both faces and symbols from EAL for each pathway (V1-rFG, V1-rpSTS). As sex[38], age[39], and brain volume[40] are known to impact brain structure and signal timing, we included these variables and their interactions with EAL as predictors in each model. Given the importance of the V1-rFG and V1-rpSTS pathways for face processing, we anticipated positive associations between N170 latency and EAL within these pathways during face but not symbol perception. We hypothesized that the association between N170 face latency and EAL along these pathways would be strongest for the typically developing control (TDC) group, indicative of a more efficient and effective face processing system. Because N170 latency is known to decrease

throughout development[26], we anticipated a negative association between age and N170 latency for all pathways, conditions, and cohorts. To identify the model best suited for predicting N170 latency for each condition (face, symbol), pathway (V1-rFG, V1-rpSTS) and cohort (total sample, TDC, ASD), we performed stepwise model selection using both forward and backward regression, which involves the addition and removal of predictors until the model with the lowest Akaike Information Criterion (AIC) is found[41].

Estimated Axonal Latency in two face processing pathways is positively associated with N170 latency to faces, not symbols

We first investigated associations between EAL and N170 latency along the V1-rFG and V1-rpSTS pathways for the total sample (Table 2, Fig. 2). For both pathways, the best fit models predicting N170 latency to faces revealed a significant positive association with EAL, and a significant negative association with age. These associations between N170 latency and EAL along both investigated face processing pathways were specific to faces. When predicting N170 latency to symbols, for both pathways, age was a significant negative predictor in the best fit models. While EAL remained a predictor for only the V1-rFG pathway, its association with N170 latency to symbols was not significant. In the total sample, brain volume and sex were never retained in any models for either pathway or condition.

Individuals with and without autism rely upon different pathways for face processing

We next investigated associations between EAL and N170 latency along the V1-rFG and V1-rpSTS pathways for each cohort separately (Table 3, Fig. 3). When predicting N170 latency to faces, we found a significant positive association with EAL in the TDC cohort for the V1-rFG pathway, but EAL was not retained for the V1-rpSTS pathway. However, we found divergent results in the ASD cohort. When predicting N170 latency to faces for the ASD cohort, EAL

within the V1-rFG pathway was not retained in the best fit model, but we found a trending positive association with EAL within the V1-rpSTS pathway. Age was a significant negative predictor in all best fit models of N170 latency to faces for both cohorts and pathways. For the ASD cohort only, sex remained an important, albeit non-significant, predictor for both pathways in these face latency models.

No variables were significant predictors of N170 latency to symbols in either cohort or pathway. While not significant, EAL was retained in the model predicting N170 latency to symbols as a trending positive association for only the TDC cohort only along the V1-rFG pathway. Age was retained as a non-significant but negative predictor of N170 latency to symbols for both cohorts and pathways. Brain volume and sex were never retained in any models predicting N170 latency to symbols.

Discussion

Neuroimaging modalities have traditionally captured proxies of brain function, such as changes in cortical blood volume or blood oxygen level dependent (BOLD) response. These measures are reflective of indirect metabolic and neurovascular demands that co-occur with functional activation at relatively low temporal resolution[42]. On the other hand, direct measures of neuronal electrical function, such as EEG, typically lack detailed spatial resolution and cannot examine the function of deep subcortical structures critical for complex behavior and implicated in disease processes. Historically, this has made it challenging to study the underlying neurophysiological correlates of disrupted cognitive function in brain disorders like ASD. For the first time, we present and validate a unified approach to estimate *in vivo* functional action potential transmission time between regions of the human brain using non-invasive, widely available, and spatially specific MRI techniques. This approach, estimated axonal latency (EAL),

utilizes classic neuroscientific models of axonal structure, particularly diameter and myelin thickness, and traditional tractography methods to provide a voxel-wise estimate of action potential transmission time between regions of the brain. To validate this measure, we evaluated the association between EAL along two well established face processing pathways and face processing speed measured via EEG. We observed specific and significant relationships between N170 latency, a well established electrophysiological metric of face processing speed, and EAL along the V1-rFG and V1-rpSTS pathways. By using adolescent populations with and without autism, we demonstrated its ability to account for differences in neuronal processing speed that occur across development and vary with disorder.

In a large, well characterized adolescent sample of both autistic and typically developing controls, EAL was specifically associated with face processing speed as measured by N170 signal latency, an association maintained across both investigated face processing pathways. In both V1-rFG and V1-rpSTS pathways, we find significant positive associations between N170 latency to faces and EAL. These results were nearly statistically identical in both the V1-rFG and V1-rpSTS pathways in the total sample, underscoring their joint importance for face processing and role in N170 signal generation[32,33]. Interestingly, the association between N170 latency and EAL was completely absent in response to non-face stimuli, demonstrating the noteworthy specificity of EAL to the investigated cognitive process along relevant pathways. The lack of a structure-function relationship during the non-specialized cognitive condition (i.e., symbol processing) may provide a structural account for the conflict resolution that must occur when the brain is deciding along which pathway to propagate a given signal when categorizing competing representations of incoming stimuli[43].

We also found that the best fit models for each condition and pathway included age as a significant negative predictor of N170 latency in the total sample. This result is not surprising, as myelination of the cortex continues throughout adolescent development[39,44]. These developmental processes increase electrophysiological signaling speed and network efficiency[40,45]. However, despite the strong effect of age, EAL remained a significant positive predictor capable of explaining variance in N170 latency to faces above and beyond that explained by age.

We next examined EAL in the context of ASD, as autistic individuals often display slower N170 latencies to faces than their TDC counterparts[29] and demonstrate white matter differences in development[6,46,47]. To investigate whether our novel structural metric of neuronal latency may account for these observed functional differences, we investigated the relationship between EAL and N170 latency in the TDC and ASD cohorts separately. For N170 latency to faces, we observed divergent results between the two groups. For the TDC cohort, we found positive associations between N170 face latency and EAL along the V1-rFG pathway. However, for ASD participants, we find only a trending positive association between EAL and N170 face latency in the V1-rpSTS pathway. While FG and pSTS are both core nodes[48] in the face processing network that enable the successful perception, interpretation, and response to faces, these regions each contribute to unique aspects of face processing[33]. The V1-rFG pathway is the canonical, shorter face processing pathway recruited for the holistic processing of human faces. Alternatively, the V1-rpSTS is a longer and perhaps less direct pathway important for the processing of facial features fundamental to expression and identity[33]. Our results demonstrate that V1-rFG EAL is a structural determinant of neural signal latency during face processing for TDC individuals only. ASD participants may instead rely upon a more diffuse network for face

processing, as V1-rpSTS EAL only weakly accounts for N170 latency in this cohort. These results provide a potential structural explanation of N170 latency delays often observed in this population.

Given our desire to account for differences in neuronal processing speed that occur in development and vary in autism, we included both sex and brain size as predictors in our models due to their documented associations with ASD[49,50] and development[39]. ASD diagnosis[51] and symptom presentation[52] have been shown to vary across sexes. For example, while females are often better able to camouflage or mask their symptoms[49,53], differences in N170 face latencies have been associated with symptom severity in females, but not males[54]. Interestingly, sex was retained in models predicting N170 latency only to faces and only in the ASD cohort. This result indicates that sex is required to account for variance in face processing speed only for ASD individuals. Despite the fact that brain size increases reliably with age[39] and that brain volume differences are consistently observed in ASD[50,55], total brain volume was not retained in any model included in our analyses. Therefore, brain size fails to account for additional variance in N170 latency above and beyond our novel EAL metric.

In calculating EAL, we used the T1-weighted/T2-weighted ratio, a widely available and easily acquired MRI metric to measure myelin content. However, there are limitations in the specificity of this metric for the quantification of myelin compared to gold standard magnetization transfer myelin quantification, particularly within deep white matter pathways[56]. However, with the significant associations between structural and functional metrics of signal latency identified in this study, we would only expect improved myelin quantification in future studies to reduce noise and improve EAL estimation. Future studies should expand upon our

foundational work to include the investigation of additional pathways, cognitive processes, developmental stages, and disorders.

Another limitation to the current work is that we performed a secondary analysis of an EEG paradigm that presents emotional faces and symbols as feedback in the context of a visual implicit learning task[36]. These stimuli were presented concurrently with task feedback text (i.e., "Right" or "Wrong"), and they differed on low level stimulus features such as spatial frequency and contrast. As such, this paradigm was not optimized to assess basic face processing, and N170 latency may have been impacted by additional ongoing cognitive processes related to the central task or processing of the co-occurring visual information. Future work can address this limitation through use of a basic face processing paradigm.

Finally, while it is a strength that we employed a multimodal imaging approach to validate our novel EAL metric, future work can further interrogate associations between the structural and electrophysiological determinants of signal speed with dual EEG-fMRI data collection. We employed a powerful meta-analytic approach to define our V1, FG, and pSTS regions of interest, but results may be further strengthened by simultaneously capturing N170 latency and defining functional regions of interest on an individual level via fMRI.

Establishing the relationship between brain structure and function has been a key, decades-old goal in cognitive neuroscience as individual differences in structural and functional networks may shape the phenotypes of neurodevelopmental disorders[57–59]. Here, we introduce EAL as a novel metric capable of quantifying the structural determinants of neuronal signal latency. For the first time, we present a structural measure of neuronal function validated by electrophysiological measurements. By combining voxel-wise estimates of neuronal conduction velocity with measures of tract length, EAL is able to provide estimates of signal latency

between any two connected regions in the brain at either the single fiber or whole-brain network level. Additionally, EAL can be derived on a single-subject level, paving the way for precision imaging estimates of individual processing time for specific cognitive functions. This approach not only allows for a deeper understanding of the normative relationship between processing speed and cognitive function, but also the ability to individually measure differences in this relationship which are often observed in heterogenous neurodevelopmental disorders like ASD. Such advancements could pave the way for predictive biomarkers of atypical neural development and inform the mechanisms underlying targeted interventions aimed at improving cognitive and social outcomes for autistic individuals. By applying this metric to known cognitive networks, EAL could advance computational simulations of the brain derived from human data by providing accurate estimates for signal transmission time. As such, EAL provides an avenue towards significant advancement in human neuroimaging as a novel *in vivo* cellular approach to understanding complex human behavior.

Methods

Participants

Here, we employ Wave 1 data collected at Seattle Children's Research Institute, the University of California Los Angeles, Harvard Medical School, and Yale University as part of the Gender Exploration of Neurogenetics and Development to Advance Autism Research (GENDAAR) consortium, supported by an NIH Autism Center of Excellence Network. Exclusion criteria for this dataset included premature birth, a known genetic condition, history of neurological disorder except uncomplicated non-focal epilepsy, active seizures within the last year, and an inability to comprehend task instructions. All participants underwent a comprehensive phenotyping process including the collection of demographic data such as sex

and age as well as confirmation of autism diagnosis for the ASD cohort. ASD and TDC participants were included in this study if they had completed the EEG implicit learning task and underwent structural and diffusion MRI (*n*=198). After completing the data preprocessing steps outlined below, 125 participants remained in the analysis with sufficient data across all required imaging modalities. Participant characteristics for this sample are detailed in Table 1.

EEG Methods

EEG Data Collection

At all four sites, EEG data were collected with the Electrical Geodesics, Inc (EGI) 128-channel Net Amps 300 system (Magstim EGI Inc., Eugene OR) with HydroCel nets using Net Station 4.4.2, 4.5.1, or 4.5.2 with a standard Net Station acquisition template. Data were sampled at 500 Hz , referenced to Cz, and impedances were kept below 50 kΩ. During their visit, participants' heads were measured and the appropriate size electrode net was applied before beginning EEG collection. Each participant was seated in front of an 80 cm monitor with a button box and researcher beside them. Participants underwent EEG while participating in a series of paradigms including an implicit learning task[36] in which they were instructed to classify abstract, fractal images into two groups. Participants were provided feedback on their performance in the form of emotional faces from the NimStim face database[60] (120 trials) and nonsocial symbols (120 trials). These feedback stimuli were matched for visual angle only. Correct responses were indicated via a happy male or female face (social) or a colored star (nonsocial) presented in the center of the screen, and the word “Right” presented at the bottom of the screen. Incorrect responses were indicated via a sad male or female face (social) or a colored “X” (nonsocial) presented in the center of the screen, and the word “Wrong” presented at the bottom of the screen.

EEG Data Processing

Data preprocessing was completed using the Automated Pipe-Line for the Estimation of Scale-wise Entropy from EEG Data[37] (APPLESEED v1.2.20240717) implemented with EEGLab v2022.1 and Matlab R2020a software (Mathworks, Natick, MA). In this pipeline, data were downsampled to 250 Hz and segmented into -100 to 1000 ms epochs time locked to feedback stimulus (face, symbol) onset. Problematic channels with excessive or flat amplitudes were removed, and then epochs were identified as artifacts and removed if (1) the experimenter indicated a trial was invalid (i.e., the participant was not attentive) during data collection, or (2) voltage exceeded 500 μV in any channel. The data were then subjected to independent component analysis, and problematic components were identified and removed using the adjusted_ADJUST algorithm[61]. On average, 24.96 components (4-62) were removed. Participants with greater than 45 components removed were excluded from further analysis (*n*=12, 6 TDC). Epochs in which the standard deviation exceeded 80 μV within a 200 ms sliding window with a 100 ms window step were then discarded as artifacts. Participants with fewer than 50 trials per condition were excluded from further analysis (*n*=22, 9 TDC). On average, 102.12 face trials (51-120) and 101.80 symbol trials (50-120) were retained. Finally, problematic channels identified via the FASTER algorithm[62] and those initially discarded as problematic were interpolated. On average, 6.08 channels (2-11) were interpolated.

N170 Latency Computation

We quantified N170 latency to faces and symbols as the time at which the maximum negative peak over 3 consecutive points occurred 170 to 270 ms after stimulus onset in parietal/occipital channels over the right hemisphere (channels 89, 90, 91, 94, 95, 96)[63–66]. Visual manual inspection confirmed successful peak identification for each participant and condition.

For the total sample, N170 latency to faces averaged 209.80 (176-268) ms, and N170 latency to symbols averaged 217.26 (172-268) ms. For the TDC cohort, N170 latency to faces averaged 206.91 (176-268) ms, and N170 latency to symbols averaged 210.67 (172-268) ms. For the ASD cohort, N170 latency to faces averaged 212.40 (180-268) ms, and N170 latency to symbols averaged 223.20 (176-268) ms. To investigate differences in N170 latency, we performed a repeated-measures ANOVA with the within-subjects factor of condition (faces, symbols) and the between-subjects factor of cohort (TDC, ASD) for the final dataset. As anticipated, this analysis revealed a significant main effect of cohort, such that TDC participants had significantly faster latencies than ASD participants ($F(1,123)=6.47$, $p=.012$), and a significant main effect of condition such that latencies to faces were significantly faster than latencies to symbols ($F(1,123)=15.44$, $p<.001$). There was also a significant interaction between cohort and condition ($F(1,123)=4.72$, $p=.032$) such that ASD participants displayed particularly slower latencies to symbols. Although grand average N170 amplitude negativity was not greater for faces with this paradigm (Fig. 1A) , only latency was of interest for the present analyses.

MRI Methods

MRI Collection

At all four sites, structural and diffusion images were acquired via a harmonized imaging protocol using either Siemens TrioTim or Prisma scanners with field strength of 3T. Diffusion images were acquired with an isotropic voxel size of $2\times2\times2mm^3$, 64 non-collinear gradient directions at b = 1000 s/mm^2, and 1 b = 0, TR = 7300ms, TE = 74ms. T1-weighted MPRAGE images were acquired with a FOV of 176×256×256, an isotropic voxel size of $1\times1\times1mm^3$, and TE = 3.3. T2-weighted images were acquired with a FOV of 128×128×34 with a voxel size of $1.5\times1.5\times4mm^3$, and TE = 35.

MRI Image Preprocessing

T1-weighted and T2-weighted images were corrected for bias fields using the N4 algorithm implemented in ANTs[67]. T1-weighted images were processed using the *recon-all* pipeline in Freesurfer[68] in order to generate volume measurements and to generate individualized brain masks. Diffusion images were preprocessed according to established protocols that have been shown to be highly reliable means of estimating white matter fiber orientation and microstructural information[69]. Images were denoised[70], corrected for Gibbs rings[71], and processed for motion correction using the *eddy* command in FSL[72] incorporating non-parametric outlier detection and replacement. Subjects were then visually checked for quality control and individuals with large errors excluded from further analysis (n=4, 1 TDC). Diffusion images were upsampled to 1.3×1.3×1.3mm isotropic voxel size to match Human Connectome Project data standards, and response functions for white matter, gray matter, and cerebrospinal fluid tissue types were generated using the *Dhollander* algorithm implemented in MRtrix3 from a subgroup of 40 randomly selected age-matched participants counter-balanced for sex and diagnosis. The fiber orientation distribution (WM-FOD) was calculated via constrained spherical deconvolution using the response functions and the MRtrix3Tissue package (https://3tissue.github.io).

Region Of Interest Selection and Creation

We defined our V1, rFG, and rpSTS regions of interest (ROIs, Fig. 1C) with a meta-analytic approach using Neurosynth.org[73]. V1, rFG, and rpSTS were chosen because of their well-established role in the facial processing network and visual processing stream[32,33]. V1 was extracted from the Neurosynth term-based meta-analysis for “primary visual,” thresholded at a z-score ≥= 3.5, and binarized. FG was extracted from the term-based meta-analysis for “ffa,”

thresholded at a z-score ≥= 12.0, binarized, and cropped to isolate the right hemisphere. pSTS was extracted from the term-based meta-analysis for "psts," thresholded at a z-score ≥= 3.5, binarized, and cropped to isolate the right hemisphere. All masks were registered to align with the T1-weighted image for each subject, and shifted anteriorly by 12 mm via linear transform to avoid overlapping the cerebellum. All cropping and thresholding was done using FSL's FSLview image editing tools and FSLmaths[72].

Tractography

Whole brain tractography was performed using MRtrix3 similar to previously published methods[74]. The WM-FOD was used to provide directional information for fiber tracking and density. The white matter/gray matter interface was determined for each subject derived from their T1-weighted image using a hybrid surface and volume approach including subcortical structures[75]. The interface was seeded with streamlines until 50,000,000 tracts successfully meeting inclusion criteria were generated. These were subsequently pruned back to 10,000,000 tracts via spherically informed filtering of tractograms (SIFT), a method to preserve anatomical fidelity by matching the density of tracts traversing each voxel to the WM-FOD lobe integral[76]. The WM-FODs were used to register each subject to the group-wise template, then to stereotaxic space[77]. The resulting warps were used to move the ROIs into subject space. Tracts were retained if the coordinates of each endpoint terminated within the ROI of interest (rFG, rpSTS) on one end and V1 on the other. Exclusion criteria removed tracts that were located in the cerebellum or crossed the corpus callosum. The overall mean length of the retained tracts was calculated via the *tckstats* command implemented in MRtrix3, which sums the distance between each component vertex along the length of each retained tract. This was performed in native space to avoid any errors arising from altering vertex distance after warping images to a common space. Participants

were excluded if no tracts were retained between the ROIs. Thirty-nine participants (20 TDC) were excluded due to no tracts remaining along the V1-rpSTS pathway, and an additional 10 participants (5 TDC) were also excluded from V1-rFG analyses due to no tracts remaining along this pathway. To investigate differences in tract length, we performed a repeated-measures ANOVA with the within-subjects factor of pathway (V1-rFG, V1-rpSTS) and the between-subjects factor of cohort (TDC, ASD). This analysis revealed a significant main effect of pathway, such that the V1-rpSTS pathway was significantly longer than the V1-rFG pathway ($F(1,117)=20.95$, $p<.001$). There was no significant effect of cohort ($F(1,117)=1.38$, $p=.243$), and no significant interaction between pathway and cohort ($F(1,117)=0.16$, $p=.686$). Voxels traversed by the retained tracts were identified and the aggregate conduction velocity within these voxels was averaged for each subject.

Estimated Axonal Latency (EAL) Calculation

G-ratio and aggregate conduction velocity are required to calculate estimated axonal latency (EAL). Both metrics were calculated according to previously published methods[6]. The aggregate g-ratio was calculated on a voxel-wise basis according to Stikov et al.[78,79] and was used according to Mohammadi & Callaghan[18], as displayed in Equation 1. As a measure of intra-axonal volume, the fiber density cross section was used as the axonal volume fraction (AVF)[80]. As a metric of myelin density, the T1-weighted/T2-weighted ratio was used as the myelin volume fraction (MVF). These metrics represent the total sums of each respective compartment across the volume of the voxel and are a volume-based equivalent to the original formulation of g as the ratio of axon diameter (d) to fiber diameter (D).

$$g = \frac{d}{D} = \sqrt{1 - \frac{MVF}{MVF+AVF}} \quad (1)$$

Aggregate conduction velocity (ACV) was calculated based on the calculations of Rushton[81] and Berman et al.[19], reiterating Rushton's calculation that conduction velocity (θ) is proportional to the length of each fiber segment (l) and that this is roughly proportional to *D,* which in turn can be defined as the ratio between *d* and the g-ratio (g). Furthering the considerations of Rushton, Berman et al. show that a value proportional to conduction velocity can be calculated using axon diameter and the g-ratio as in equation 2[19]:

$$\theta \; \alpha \; l \; \alpha \; Dg\sqrt{-\; ln(g)} \; \alpha \; d\sqrt{-\; ln(g)} \quad (2)$$

To investigate differences in aggregate conduction velocity, we performed a repeated-measures ANOVA with the within-subjects factor of pathway (V1-rFG, V1-rpSTS) and the between-subjects factor of cohort (TDC, ASD). This analysis revealed a significant main effect of pathway, such that aggregate conduction velocity was significantly faster along the V1-rpSTS pathway ($F(1,117)=39.96$, $p<.001$). There was no significant effect of cohort ($F(1,117)=0.81$, $p=.370$), and no significant interaction between pathway and cohort ($F(1,117)=0.03$, $p=.853$).

Finally, EAL is calculated according to equation 3, which is derived from the equation for average velocity, a well-known relationship in classical physics.

$$t = \frac{x}{\bar{v}} \rightarrow t_{conduction} = \frac{l_{axon}}{\theta} \rightarrow EAL = \frac{\overline{L_{tract}}}{ACV} \quad (3)$$

It has often been assumed that action potentials propagate down axons at roughly a constant speed[2]. Thus, we can relate the conduction velocity of an action potential to the axonal length and conduction latency. The aggregate conduction velocity of a given tract is proportional to its true conduction velocity, allowing us to substitute axonal length with mean tract length and

conduction latency with theoretical latency. As a result, EAL should be proportional to conduction latency along a given tract.

To investigate differences in EAL, we performed a repeated-measures ANOVA with the within-subjects factor of pathway (V1-rFG, V1-rpSTS) and the between-subjects factor of cohort (TDC, ASD). This analysis revealed no significant effect of pathway ($F(1,117)<0.01$, $p=.958$), no significant effect of cohort ($F(1,117)=0.09$, $p=.769$), and no significant interaction between pathway and cohort ($F(1,117)=0.05$, $p=.831$).

Stepwise Model Selection

In order to identify the model best suited for predicting N170 latency across cohorts (total sample, TDC, ASD), pathways (V1-rFG, V1-rpSTS), and conditions (faces, symbols), we performed stepwise model selection using both forward and backward regression, which involves the addition and removal of predictors until the model with the lowest AIC criterion is found. Model selection was conducted using R 4.2.3[82] with the stepAIC function from the MASS package[83]. Our models included seven predictors: EAL, sex, age, total brain volume, and the interactions between EAL and each of the other predictors. We identified the best fit model as the model with the lowest AIC value before an intercept-only model. Finally, a general linear model was run on the predictors remaining in the best fit model to determine the direction and significance of its association with N170 latency.

Acknowledgments

Funding for this work was provided by the NIH R01 MH100028 to K.A.P. and NIH K01 MH125173 to M.P.H.

Author Contributions

All data were collected by the Gender Exploration of Neurogenetics and Development to Advance Autism Research (GENDAAR) consortium. C.R.C. and M.G.N. contributed equally as first authors. B.T.N. and M.H.P. contributed equally as senior authors. C.R.C., M.G.N., B.T.N., and M.H.P. conceptualized the project, analyzed the data, and wrote the manuscript. Z.J. stored and organized the data. J.V.H., K.A.P, T.J.D., B.T.N., and M.H.P. provided project supervision. All authors provided critical feedback on the manuscript and approved the final draft.

Figures

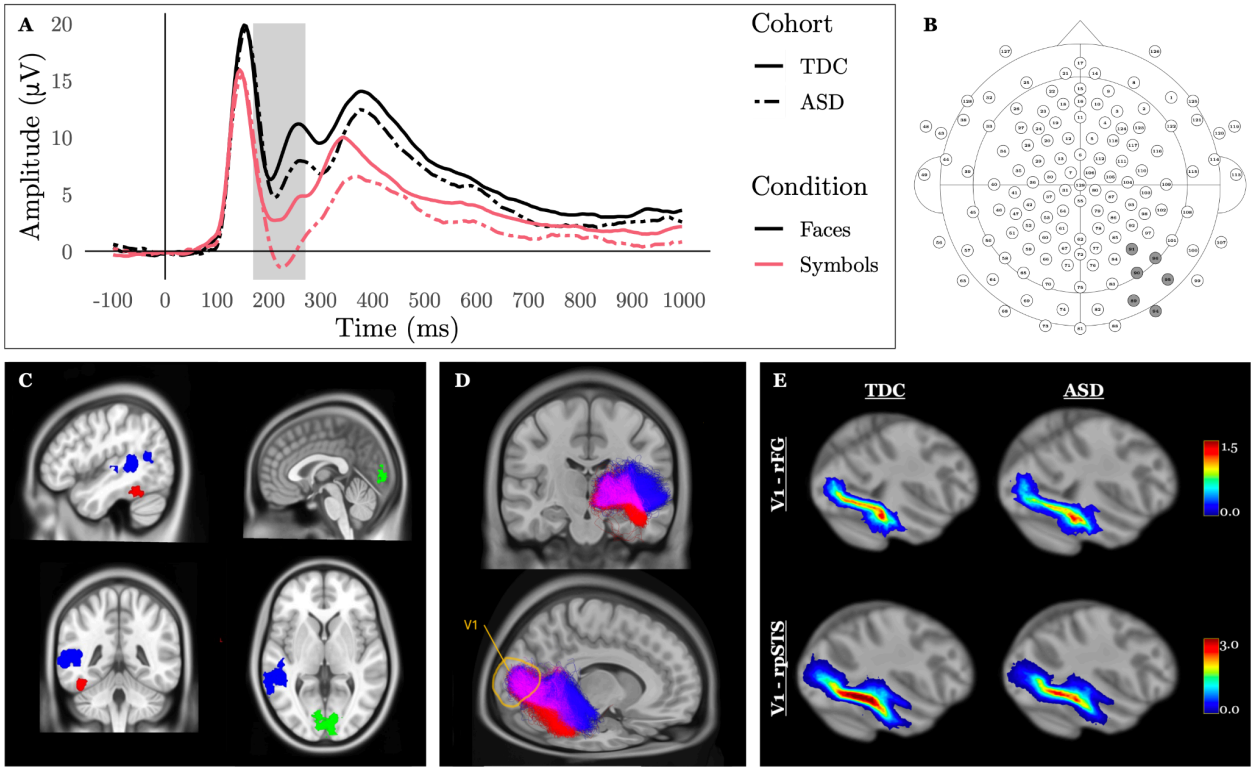

Fig. 1: A multimodal investigation of the relationship between electrical function and axonal structure during face processing. A) To measure EEG-based electrical function during face processing, TDC (solid line) and ASD (dashed line) participants underwent EEG during the perception of faces (black) and symbols (pink). We computed N170 latency as the negative peak latency 170-270 ms after stimulus onset (grey shading). **B)** We extracted N170 latency from right posterior/occipital (shaded) channels. **C)** To extract MRI-based axonal microstructure, we generated regions of interest including primary visual cortex (V1, green), right fusiform gyrus (rFG, red), and right posterior superior temporal sulcus (rpSTS, blue) using a meta-analytic approach. **D)** Axonal microstructure was measured along two pathways, V1-rFG (red) and V1-rpSTS (blue). Overlapping tracts are pictured in magenta. **E)** Mean aggregate conduction velocity maps along all tracts retained in the study are separated by diagnostic group and tract. To create each map, voxels traversed by a retained tract were summed across all participants in a group, then divided by the total number of participants for a representation of within-group tract cohesiveness and overall conduction velocity.

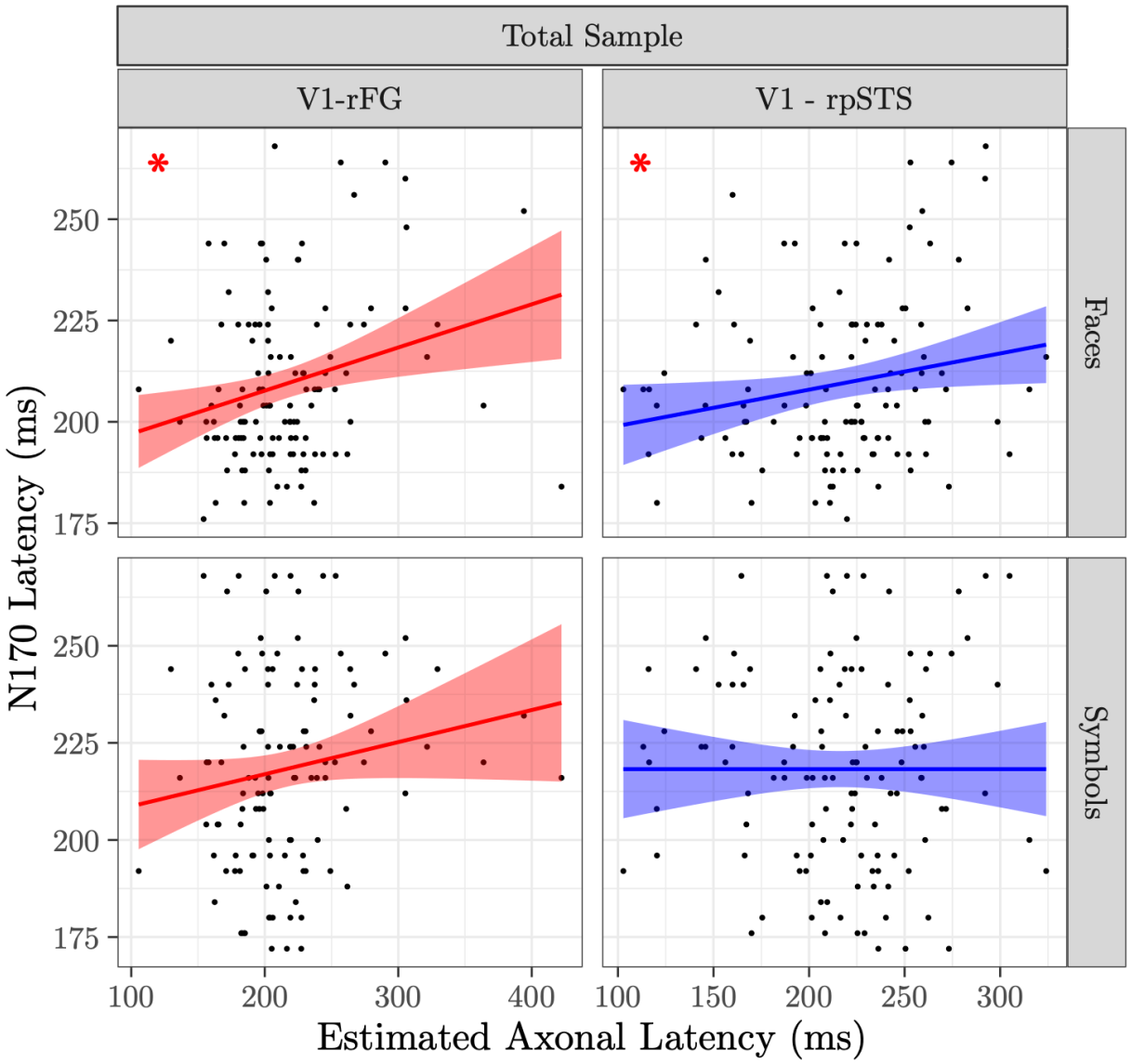

Fig. 2: Associations between estimated axonal latency and N170 latency are specific to face processing along relevant pathways. The relationship between estimated axonal latency (EAL) and N170 latency is plotted for each pathway (red, V1-rFG; blue, V1-rpSTS) and each condition (faces, symbols) for the total sample (*N*=125). Results reveal a significant positive association between EAL and N170 latency across both pathways only in the faces condition. Significant associations are indicated via red asterisk. V1, primary visual cortex; rFG, right fusiform gyrus; rpSTS, right posterior superior temporal sulcus.

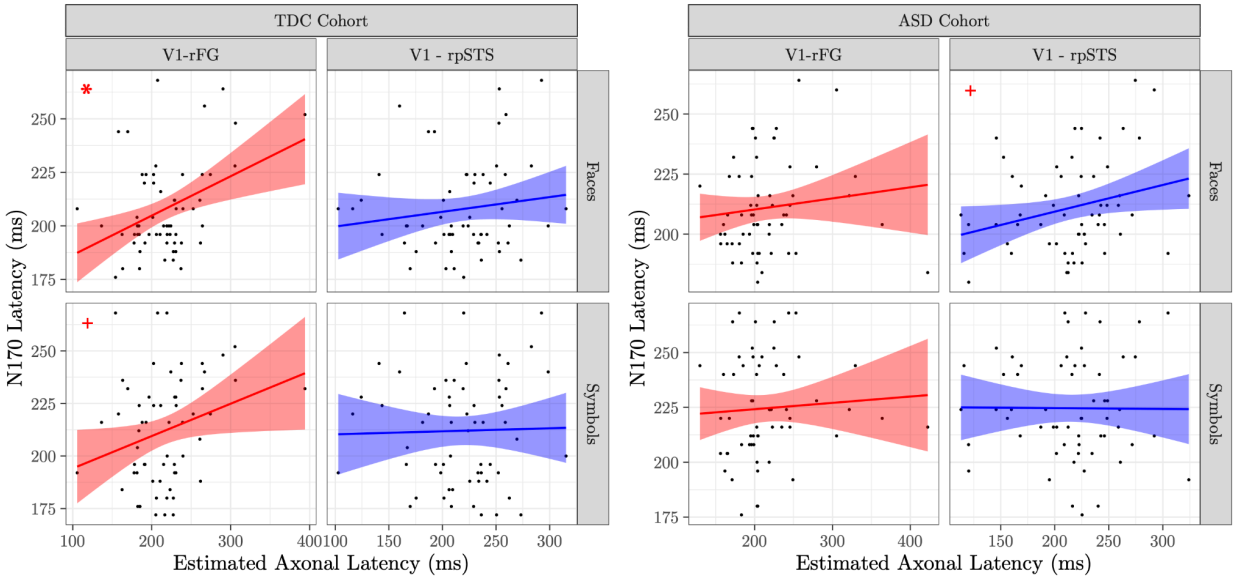

Fig. 3: Estimated axonal latency is positively associated with N170 latency in different pathways for individuals with and without autism. The relationship between estimated axonal latency (EAL) and N170 latency is plotted for each pathway and each condition (faces, symbols) for the TDC cohort (*N*=63, left) and the ASD cohort (*N*=62, right). For TDC participants, we find EAL is positively associated with N170 latency to faces along only the V1-rFG pathway (red). For ASD participants, EAL is trending towards a positive association with N170 latency to faces along only the V1-rpSTS pathway (blue). Significant associations are indicated via red asterisk. Trending associations are indicated via red +. TDC, typically developing control; ASD, autism spectrum disorder; V1, primary visual cortex; rFG, right fusiform gyrus; rpSTS, right posterior superior temporal sulcus.

Tables

Demographic		Total Sample	TDC Cohort	ASD Cohort
Age (Years)	Range	8.08 - 17.92	8.08-17.92	8.17 - 17.83
	Mean	12.95	13.16	12.74
	Std. Deviation	2.97	3.02	2.92
	Group Difference	$t(123) = 0.80$, $p = .423$		
Sex (N)	Male	68	33	35
	Female	57	30	27
	Total	125	63	62
	Group Difference	$X^2(1, N = 125) = 0.08$, $p = .782$		
Total brain volume (mm)	Range	883847-1731175	912468-1452518	883847-1731175
	Mean	1206619	1205468	1207789
	Std. Deviation	124060.4	114255.4	134221.9
	Group Difference	$t(123) = -0.14$, $p = .917$		

Table 1: Participant Demographics. Demographic information was recorded at each site. Total brain volume measurements were obtained from T1-weighted images. There are no significant group differences across TDC and ASD cohorts for any of our considered demographic variables. A two-way ANOVA revealed no statistically significant interaction between diagnostic group and sex for age ($F(1,121)=0.24$, $p=.626$) or total brain volume ($F(1,121)=0.04$, $p=.846$).

Condition	Pathway	Adjusted R^2	Estimated Axonal Latency	Age	Sex	Brain Volume
Faces	V1 - rFG	.21	***b* = 0.08, *p* = .023**	***b* = -0.24, *p* < .001**	-	-
	V1 - rpSTS	.21	***b* = 0.08, *p* = .022**	***b* = -0.24, *p* < .001**	-	-
Symbols	V1 - rFG	.04	*b* = 0.07, *p* = .162	***b* = -0.13, *p* = .043**	-	-
	V1 - rpSTS	.04	-	***b* = -0.16, *p* = .015**	-	-

Table 2: Results of the best fit models predicting N170 latency for the total sample. A stepwise regression analysis revealed the best fit model for each condition and pathway in the total cohort by identifying the model with the lowest AIC value. Significant predictors are indicated via boldface font. Predictors that were not retained in the best fit model are indicated via hyphen.

Condition	Cohort	Pathway	Adjusted R^2	Estimated Axonal Latency	Age	Sex	Brain Volume
Faces	TDC	V1 - rFG	.29	***b* = 0.15, *p* <.001**	***b* = -0.25, *p* < .001**	-	-
		V1 - rpSTS	.21	-	***b* = -0.27, *p* < .001**	-	-
	ASD	V1 - rFG	.17	-	***b* = -0.22, *p* = .001**	*b* = 7.61, *p* = .105	-
		V1 - rpSTS	.20	*b = 0.09, p = .065*	***b* = -0.20, *p* < .001**	*b* = 6.5, *p* = .140	-
Symbols	TDC	V1 - rFG	.08	*b = 0.13, p = .073*	*b* = -0.14, *p* = .130	-	-
		V1 - rpSTS	.04	-	*b = -0.17, p = .053*	-	-
	ASD	V1 - rFG	.08	-	*b* = -0.14, *p* = .130	-	-
		V1 - rpSTS	.01	-	*b* = -0.11, *p* = .211	-	-

Table 3: Results of the best fit models predicting N170 latency for the TDC and ASD cohorts. A stepwise regression analysis revealed the best fit model for each condition and pathway in the TDC and ASD cohorts by identifying the model with the lowest AIC value. Significant predictors are indicated via boldface font. Trending significant predictors are indicated via italicized font. Predictors that were not retained in the best fit model are indicated via hyphen.

References

1. Muzio, M. R., Fakoya, A. O. & Cascella, M. Histology, Axon. in *StatPearls* (StatPearls Publishing, Treasure Island (FL), 2025).
2. Hodgkin, A. L. & Huxley, A. F. A quantitative description of membrane current and its application to conduction and excitation in nerve. *J. Physiol.* **117**, 500–544 (1952).
3. Häusser, M. The Hodgkin-Huxley theory of the action potential. *Nat. Neurosci.* **3**, 1165–1165 (2000).
4. Khelfaoui, H., Ibaceta-Gonzalez, C. & Angulo, M. C. Functional myelin in cognition and neurodevelopmental disorders. *Cell. Mol. Life Sci. CMLS* **81**, 181 (2024).
5. Duncan, I. D. & Radcliff, A. B. Inherited and acquired disorders of myelin: The underlying myelin pathology. *Exp. Neurol.* **283**, 452–475 (2016).
6. Newman, B. T. *et al.* Conduction velocity, G-ratio, and extracellular water as microstructural characteristics of autism spectrum disorder. *PLOS ONE* **19**, e0301964 (2024).
7. Dimond, D. *et al.* Reduced White Matter Fiber Density in Autism Spectrum Disorder. *Cereb. Cortex N. Y. N 1991* **29**, 1778–1788 (2019).
8. Zikopoulos, B. & Barbas, H. Changes in Prefrontal Axons May Disrupt the Network in Autism. *J. Neurosci.* **30**, 14595–14609 (2010).
9. Berry, C. M., Grundfest, H. & Hinsey, J. C. The electrical activity of regenerating nerves in the cat. *J. Neurophysiol.* **7**, 103–115 (1944).
10. Hursh, J. B. Conduction velocity and diameter of nerve fibers. *Am. J. Physiol.-Leg. Content* **127**, 131–139 (1939).
11. Travers, B. G. *et al.* Longitudinal processing speed impairments in males with autism and the effects of white matter microstructure. *Neuropsychologia* **53**, 137–145 (2014).

12. Beres, A. M. Time is of the Essence: A Review of Electroencephalography (EEG) and Event-Related Brain Potentials (ERPs) in Language Research. *Appl. Psychophysiol. Biofeedback* **42**, 247 (2017).
13. Zhang, H. *et al.* The applied principles of EEG analysis methods in neuroscience and clinical neurology. *Mil. Med. Res.* **10**, 67 (2023).
14. Holdsworth, S. J. & Bammer, R. Magnetic Resonance Imaging Techniques: fMRI, DWI, and PWI. *Semin. Neurol.* **28**, 395–406 (2008).
15. Ebrahimzadeh, E. *et al.* Simultaneous electroencephalography-functional magnetic resonance imaging for assessment of human brain function. *Front. Syst. Neurosci.* **16**, (2022).
16. Coleman, C. & Van Horn, J. D. Towards Comprehensive Connectivity Modeling. *Neuroinformatics* **22**, 225–227 (2024).
17. Campbell, J. S. W. *et al.* Promise and pitfalls of g-ratio estimation with MRI. *NeuroImage* **182**, 80–96 (2018).
18. Mohammadi, S. & Callaghan, M. F. Towards in vivo g-ratio mapping using MRI: Unifying myelin and diffusion imaging. *J. Neurosci. Methods* **348**, 108990 (2021).
19. Berman, S., Filo, S. & Mezer, A. A. Modeling conduction delays in the corpus callosum using MRI-measured g-ratio. *NeuroImage* **195**, 128–139 (2019).
20. Pascalis, O. *et al.* Development of Face Processing. *Wiley Interdiscip. Rev. Cogn. Sci.* **2**, 666–675 (2011).
21. Pascalis, O. & Kelly, D. J. The Origins of Face Processing in Humans: Phylogeny and Ontogeny. *Perspect. Psychol. Sci. J. Assoc. Psychol. Sci.* **4**, 200–209 (2009).
22. Golarai, G., Grill-Spector, K. & Reiss, A. L. Autism and the development of face processing.

Clin. Neurosci. Res. **6**, 145–160 (2006).

23. Eimer, M. The Face-Sensitivity of the N170 Component. *Front. Hum. Neurosci.* **5**, 119 (2011).
24. Bentin, S., Allison, T., Puce, A., Perez, E. & McCarthy, G. Electrophysiological Studies of Face Perception in Humans. *J. Cogn. Neurosci.* **8**, 551–565 (1996).
25. Rossion, B. & Jacques, C. The N170: Understanding the time course of face perception in the human brain. in *The Oxford handbook of event-related potential components* 115–141 (Oxford University Press, New York, NY, US, 2012).
26. Miki, K., Honda, Y., Takeshima, Y., Watanabe, S. & Kakigi, R. Differential age-related changes in N170 responses to upright faces, inverted faces, and eyes in Japanese children. *Front. Hum. Neurosci.* **9**, (2015).
27. McPartland, J., Dawson, G., Webb, S. J., Panagiotides, H. & Carver, L. J. Event-related brain potentials reveal anomalies in temporal processing of faces in autism spectrum disorder. *J. Child Psychol. Psychiatry* **45**, 1235–1245 (2004).
28. Hudac, C. M. & Webb, S. J. EEG Biomarkers for Autism: Rational, Support, and the Qualification Process. *Adv. Neurobiol.* **40**, 545–576 (2024).
29. Kang, E. *et al.* Atypicality of the N170 Event-Related Potential in Autism Spectrum Disorder: A Meta-Analysis. *Biol. Psychiatry Cogn. Neurosci. Neuroimaging* **3**, 657–666 (2018).
30. Parker, T. C. *et al.* The N170 event-related potential reflects delayed neural response to faces when visual attention is directed to the eyes in youths with ASD. *Autism Res. Off. J. Int. Soc. Autism Res.* **14**, 1347–1356 (2021).
31. Vettori, S., Jacques, C., Boets, B. & Rossion, B. Can the N170 Be Used as an

Electrophysiological Biomarker Indexing Face Processing Difficulties in Autism Spectrum Disorder? *Biol. Psychiatry Cogn. Neurosci. Neuroimaging* **4**, 321–323 (2019).

32. Wang, X. *et al.* The Hierarchical Structure of the Face Network Revealed by Its Functional Connectivity Pattern. *J. Neurosci.* **36**, 890–900 (2016).
33. Wang, Y. *et al.* Multimodal Mapping of the Face Connectome. *Nat. Hum. Behav.* **4**, 397 (2020).
34. Gao, C., Conte, S., Richards, J. E., Xie, W. & Hanayik, T. The neural sources of N170: Understanding timing of activation in face-selective areas. *Psychophysiology* **56**, e13336 (2019).
35. Deffke, I. *et al.* MEG/EEG sources of the 170-ms response to faces are co-localized in the fusiform gyrus. *NeuroImage* **35**, 1495–1501 (2007).
36. Scott-Van Zeeland, A. A., Dapretto, M., Ghahremani, D. G., Poldrack, R. A. & Bookheimer, S. Y. Reward Processing in Autism. *Autism Res. Off. J. Int. Soc. Autism Res.* **3**, 53–67 (2010).
37. Puglia, M. H., Slobin, J. S. & Williams, C. L. The automated preprocessing pipe-line for the estimation of scale-wise entropy from EEG data (APPLESEED): Development and validation for use in pediatric populations. *Dev. Cogn. Neurosci.* **58**, 101163 (2022).
38. Wang, Y. *et al.* Sex differences in white matter development during adolescence: A DTI study. *Brain Res.* **1478**, 1–15 (2012).
39. Lebel, C. & Deoni, S. The Development of Brain White Matter Microstructure. *NeuroImage* **182**, 207–218 (2018).
40. Buzsáki, G., Logothetis, N. & Singer, W. Scaling Brain Size, Keeping Timing: Evolutionary Preservation of Brain Rhythms. *Neuron* **80**, 751 (2013).

41. Portet, S. A primer on model selection using the Akaike Information Criterion. *Infect. Dis. Model.* **5**, 111–128 (2020).

42. Glover, G. H. Overview of Functional Magnetic Resonance Imaging. *Neurosurg. Clin. N. Am.* **22**, 133–139 (2011).

43. Aron, A. R. The neural basis of inhibition in cognitive control. *Neurosci. Rev. J. Bringing Neurobiol. Neurol. Psychiatry* **13**, 214–228 (2007).

44. Newman, B. T., Patrie, J. T. & Druzgal, T. J. An intracellular isotropic diffusion signal is positively associated with pubertal development in white matter. *Dev. Cogn. Neurosci.* **63**, 101301 (2023).

45. Purves, D. *et al.* Increased Conduction Velocity as a Result of Myelination. in *Neuroscience. 2nd edition* (Sinauer Associates, 2001).

46. Nickel, K. *et al.* Altered transcallosal fiber count and volume in high-functioning adults with autism spectrum disorder. *Psychiatry Res. Neuroimaging* **322**, 111464 (2022).

47. Wilkinson, M., Wang, R., van der Kouwe, A. & Takahashi, E. White and gray matter fiber pathways in autism spectrum disorder revealed by ex vivo diffusion MR tractography. *Brain Behav.* **6**, e00483 (2016).

48. Haxby, J. V. *et al.* The distributed human neural system for face perception. *Trends Cogn. Sci.* **4**, 223–233 (2000).

49. Napolitano, A. *et al.* Sex Differences in Autism Spectrum Disorder: Diagnostic, Neurobiological, and Behavioral Features. *Front. Psychiatry* **13**, (2022).

50. Freitag, C. M. *et al.* Total Brain Volume and Corpus Callosum Size in Medication-Naïve Adolescents and Young Adults with Autism Spectrum Disorder. *Biol. Psychiatry* **66**, 316–319 (2009).

51. Loomes, R., Hull, L. & Mandy, W. P. L. What Is the Male-to-Female Ratio in Autism Spectrum Disorder? A Systematic Review and Meta-Analysis. *J. Am. Acad. Child Adolesc. Psychiatry* **56**, 466–474 (2017).
52. Ochoa-Lubinoff, C., Makol, B. A. & Dillon, E. F. Autism in Women. *Neurol. Clin.* **41**, 381–397 (2023).
53. Hull, L., Petrides, K. V. & Mandy, W. The Female Autism Phenotype and Camouflaging: a Narrative Review. *Rev. J. Autism Dev. Disord.* **7**, 306–317 (2020).
54. Coffman, M. C., Anderson, L. C., Naples, A. J. & McPartland, J. C. Sex Differences in Social Perception in Children with ASD. *J. Autism Dev. Disord.* **45**, 589–599 (2015).
55. Vaccarino, F. M. & Smith, K. M. Increased brain size in autism—what it will take to solve a mystery. *Biol. Psychiatry* **66**, 313–315 (2009).
56. Sandrone, S. *et al.* Mapping myelin in white matter with T1-weighted/T2-weighted maps: discrepancy with histology and other myelin MRI measures. *Brain Struct. Funct.* **228**, 525–535 (2023).
57. Sokolowski, H. M. & Levine, B. Common neural substrates of diverse neurodevelopmental disorders. *Brain* **146**, 438–447 (2023).
58. Soman, S. M. *et al.* Functional and structural brain network development in children with attention deficit hyperactivity disorder. *Hum. Brain Mapp.* **44**, 3394–3409 (2023).
59. Rudie, J. D. *et al.* Altered functional and structural brain network organization in autism. *NeuroImage Clin.* **2**, 79–94 (2012).
60. Tottenham, N. *et al.* The NimStim set of facial expressions: Judgments from untrained research participants. *Psychiatry Res.* **168**, 242 (2009).
61. Leach, S. C. *et al.* Adjusting ADJUST: Optimizing the ADJUST Algorithm for Pediatric

Data Using Geodesic Nets. *Psychophysiology* **57**, e13566 (2020).

62. Nolan, H., Whelan, R. & Reilly, R. B. FASTER: Fully Automated Statistical Thresholding for EEG artifact Rejection. *J. Neurosci. Methods* **192**, 152–162 (2010).
63. Webb, S. J. *et al.* Identifying Age Based Maturation in the ERP Response to Faces in Children With Autism: Implications for Developing Biomarkers for Use in Clinical Trials. *Front. Psychiatry* **13**, 841236 (2022).
64. Rutherford, H. J. V. *et al.* Intranasal oxytocin and the neural correlates of infant face processing in non-parent women. *Biol. Psychol.* **129**, 45–48 (2017).
65. Malak, S. M., Crowley, M. J., Mayes, L. C. & Rutherford, H. J. V. Maternal anxiety and neural responses to infant faces. *J. Affect. Disord.* **172**, 324–330 (2015).
66. Webb, S. J. *et al.* The Autism Biomarkers Consortium for Clinical Trials: Initial Evaluation of a Battery of Candidate EEG Biomarkers. *Am. J. Psychiatry* **180**, 41–49 (2023).
67. Avants, B., Tustison, N. J. & Song, G. Advanced Normalization Tools: V1.0. *Insight J.* (2009) doi:10.54294/uvnhin.
68. Fischl, B. FreeSurfer. *NeuroImage* **62**, 774–781 (2012).
69. Newman, B. T., Dhollander, T., Reynier, K. A., Panzer, M. B. & Druzgal, T. J. Test-retest reliability and long-term stability of 3-tissue constrained spherical deconvolution methods for analyzing diffusion MRI data. *Magn. Reson. Med.* **84**, 2161–2173 (2020).
70. Veraart, J. *et al.* Denoising of diffusion MRI using random matrix theory. *NeuroImage* **142**, 394–406 (2016).
71. Kellner, E., Dhital, B., Kiselev, V. G. & Reisert, M. Gibbs-ringing artifact removal based on local subvoxel-shifts. *Magn. Reson. Med.* **76**, 1574–1581 (2016).
72. Smith, S. M. *et al.* Advances in functional and structural MR image analysis and

implementation as FSL. *NeuroImage* **23 Suppl 1**, S208-219 (2004).

73. Yarkoni, T., Poldrack, R. A., Nichols, T. E., Van Essen, D. C. & Wager, T. D. Large-scale automated synthesis of human functional neuroimaging data. *Nat. Methods* **8**, 665–670 (2011).
74. Skyberg, A. M. *et al.* An epigenetic mechanism for differential maturation of amygdala–prefrontal connectivity in childhood socio-emotional development. *Transl. Psychiatry* **13**, 91 (2023).
75. Smith, R., Skoch, A., Bajada, C. J., Caspers, S. & Connelly, A. Hybrid surface-volume segmentation for improved anatomically-constrained tractography. (2020).
76. Smith, R. E., Tournier, J.-D., Calamante, F. & Connelly, A. SIFT: Spherical-deconvolution informed filtering of tractograms. *NeuroImage* **67**, 298–312 (2013).
77. Newman, B. T., Untaroiu, A. & Druzgal, T. J. A novel diffusion registration method with the NTU-DSI-122 template to transform free water signal fraction maps to stereotaxic space. in *ResearchGate* (2020).
78. Stikov, N. *et al.* Bound pool fractions complement diffusion measures to describe white matter micro and macrostructure. *NeuroImage* **54**, 1112–1121 (2011).
79. Stikov, N. *et al.* In vivo histology of the myelin g-ratio with magnetic resonance imaging. *NeuroImage* **118**, 397–405 (2015).
80. Raffelt, D. *et al.* Apparent Fibre Density: a novel measure for the analysis of diffusion-weighted magnetic resonance images. *NeuroImage* **59**, 3976–3994 (2012).
81. Rushton, W. A. H. A theory of the effects of fibre size in medullated nerve. *J. Physiol.* **115**, 101–122 (1951).
82. R Core Team. R: A Language and Environment for Statistical Computing. (2023).

83. Venables, W. N. & Ripley, B. D. *Modern Applied Statistics with S*. (Springer, New York, NY, 2002). doi:10.1007/978-0-387-21706-2.